DIRECT NUMERICAL SIMULATION OF TURBULENCE RADIATION INTERACTIONS IN NON-GREY MEDIA

S. Silvestri[1,*] D.J.E.M. Roekaerts[1,2] R. Pecnik[1]
[1]Department of Process and Energy Technology, Delft University of Technology, Delft, the Netherlands
[2]Department of Mechanical Engineering, Eindhoven University of Technology, Eindhoven, the Netherlands
[*] email: s.silvestri@tudelft.nl, phone: +31626345924

ABSTRACT. The present work deals with the characterization of Turbulence Radiation Interactions (TRI) in a turbulent flow of a non-grey absorbing-emitting participating media (specifically water vapour). Direct Numerical Simulation coupled with a fast Monte Carlo implementation on GPU's and a narrow band correlated-K spectral discretization is used to investigate the influence of a real gas spectrum in the modification of TRI. The results are compared with previous simulations that employed the Finite Volume Method (FVM) and a grey approximation with the use of the Planck mean absorption coefficient of water vapour. The results show that it is possible to distinguish a qualitative TRI (i.e., the modification of rms profiles and the preferential impact of TRI on different temperature scales) and a quantitative TRI (i.e., the influence of radiative term over other temperature variance budgets) and, in a real gas, the qualitative effect can be compared to a grey gas with $\kappa > \kappa_P$, due to the discrepancy between the spectral wavelength of emission and incident radiation fluctuations.

INTRODUCTION

When dealing with high temperature applications, radiation is the most significant mode of heat transfer. Therefore, it is important to understand the interaction of the three heat transfer mechanisms in high temperature radiative flows. Several numerical studies and experimental investigations have observed the appearance of interactions between the turbulent temperature field (i.e., the fluctuations of temperature and internal energy) and radiation in turbulent flows of participating media, which cause a strong heat transfer modification. These interactions lead to the appearance of a fluctuating radiative field which, in turn, acts as source/sink for quantities such as temperature variance and turbulent heat transfer. Therefore, two different aspects of turbulence radiation interactions can be studied, namely the influence of the turbulent temperature field in the modification of radiative heat transfer and the effects of radiation on the temperature statistics. Most of the studies performed on the topic deal with the first aspect [1,2,3,4]. Particularly in reactive flows, where, due to the high levels of temperature fluctuations, $\overline{T^4} \neq \overline{T}^4$. This causes a discrepancy between the radiative quantities calculated with the mean and the instantaneous temperature which can be as high as 30% [3]. More recently, also the influence of radiative heat transfer on turbulent temperature field has been investigated with the aid of DNS in different conditions [5,6,7,8,9]. The general conclusion is that the fluctuations of radiative power cause a reduction of temperature variance and, therefore, a reduction of the turbulent heat flux.
A recent study [10] analyzed the effect of radiative heat transfer on temperature structures in a fully developed turbulent channel flow using the grey gas approximation to show the influence of optical thickness (τ) in the modification of the turbulent temperature field. The results showed that, not only the magnitude of TRI changes drastically upon increasing τ, but also the behaviour of the TRI changes due to the shortening of radiative length scales. Radiative power fluctuations (Q_r'), which tend to

reduce temperature variance, behave as emission fluctuations if τ is low ($Q'_r \propto E'_m \gg G'$), while, for a large τ, also incident radiation fluctuations play a role ($Q'_r \propto E'_m - G' \ll E'_m \approx G'$). In particular, for a high enough optical thickness, incident radiation length scales correlate tighter with temperature structures enabling a recovery of temperature fluctuations that begins from larger scales. The aim of this study is to investigate the changes in TRI due to a real gas absorption spectrum. The studied case is a fully developed turbulent channel flow with isothermal boundary conditions, to enable the comparison with previous grey gas results. The lower wall has a temperature of $955\ K$, while the upper wall is at $573\ K$. The employed medium is water vapour at $1\ atm$, which is characterized by a Planck mean absorption coefficient in the range of 4 to $20\ m^{-1}$. The half channel height has been chosen to be $1\ m$ to ensure a large enough optical thickness.

GOVERNING EQUATIONS

The governing equations for a variable density absorbing-emitting turbulent flow are displayed below. We employed a low-Mach number approximation, which neglects the presence of an acoustic field. The asterisk * stands for dimensional variables, while variables without asterisk are non-dimensional:

$$\partial_t \rho + \nabla \cdot (\rho \boldsymbol{u}) = 0$$

$$\partial_t (\rho \boldsymbol{u}) + \nabla \cdot (\rho \boldsymbol{u} \otimes \boldsymbol{u}) = -\nabla \cdot p\boldsymbol{I} + \nabla \cdot \boldsymbol{\tau}$$

$$\partial_t (\rho\theta) + \nabla \cdot (\rho\theta \boldsymbol{u}) = (RePr)^{-1} \nabla^2 \theta - (RePrPl)^{-1} Q_r$$

where $\boldsymbol{\tau} = Re^{-1}(\nabla \boldsymbol{u} + (\nabla \boldsymbol{u})^T - 2/3(\nabla \cdot \boldsymbol{u})\boldsymbol{I})$ and $\rho = T_0/(T_0 + \theta)$. Note that, since λ^* , c_p^* and μ^* are constant, they have been incorporated in the definitions of Re and Pr, and removed from the governing equations. The RTE and the divergence of the heat flux depend on a non-dimensional absorption coefficient κ that varies throughout the channel. Scattering has been neglected in the description of radiative heat transfer:

$$\boldsymbol{s} \cdot \nabla I_\lambda = \kappa_\lambda (I_{b\lambda} - I_\lambda) \ ,$$

$$Q_r = \int_0^\infty \kappa_\lambda \left(4 I_{b\lambda} - \frac{1}{\pi} \int_{4\pi} I_\lambda d\Omega \right) \ ,$$

non-dimensional variables are defined as follows: space $\boldsymbol{x} = \boldsymbol{x}^* (\delta^*)^{-1}$, time $t = t^* U_b^* (\delta^*)^{-1}$, velocity $\boldsymbol{u} = \boldsymbol{u}^* (U_b^*)^{-1}$, pressure $p = p^* (\rho_c^* U_b^{*2})^{-1}$, temperature $\theta = (T^* - Tc^*)(T_h^* - Tc^*)^{-1}$, intensities $I_{b,\lambda} = I_{b,\lambda}^* \pi (\sigma^* T_c^{*4})^{-1}$, $I_\lambda = I_\lambda^* \pi (\sigma^* T_c^{*4})^{-1}$and absorption coefficient $\kappa_\lambda = \kappa_\lambda^* \delta^*$. Where indices c and h stand for cold and hot wall, while b defines a bulk quantity. The non-dimensional parameters, Reynolds, Prandtl and Planck number have a fixed value of

$$Re = \frac{U_b^* \delta^* \rho_c^*}{\mu^*} = 3750, \quad Pr = \frac{\mu^* c_p^*}{\lambda^*} = 1, \quad Pl = \frac{\lambda^* \Delta T^*}{\sigma^* T_c^{*4} \delta^*} = 0.03.$$

The reference temperatures are $T_c^* = 573\ K$ and $T_h^* = 955\ K$.

NUMERICAL IMPLEMENTATION

The computational domain is as follows: streamwise length $L_x = 4\pi\delta^*$, spanwise length $L_z = 3/2\pi\delta^*$ and wall normal height $L_y = 2\delta^*$, where δ^* is the half channel height. The number of used grid points is $192 \times 192 \times 192$. The channel is periodic in the streamwise and spanwise direction. The Navier-Stokes equations have been solved using a pseudo-spectral method in the periodic

directions, and a sixth order staggered compact finite difference scheme for the discretization of derivatives in the wall normal direction. A pressure correction scheme is applied based on the projection method, while a pressure gradient is applied in the streamwise direction in order to maintain a constant Reynolds number. For details and validation of the DNS code the reader is referred to [11,12]. For the real gas case, the radiative transfer equation has been solved with an optimized emission based reciprocal Monte Carlo formulation as described in [13]. The spectral description has been treated with a narrow band correlated-K formulation based on line-by-line spectra obtained from the HITRAN 2012 spectroscopy database [15]. The full spectra in the $500 - 1010\ K$ temperature range (with a step of $10\ K$) have been divided into 119 narrow bands with 16 quadrature points each, yielding a total of 1904×52 pseudo-spectral points. The pseudo-spectral are chosen within the Monte Carlo framework by the drawing of two random numbers (one for the band, one for the quadrature). The total number of energy bundles per cell is set to 6000, as the associated intrinsic variance results being lower than 1%. The Monte Carlo solver is executed on GPU's, implemented via the programming language CUDA. Several techniques are employed in order to increase the level of parallelization and improve the efficiency of memory access and thread execution.

VALIDATION

The validation presented hereafter will pertain only the Monte Carlo GPU solver, as the Navier-Stokes solver has been used and validated already [11]. Moreover, the details of the finite volume method employed for the grey cases are presented in [10]. The implementation of the Monte Carlo solver is verified for the grey gas cases in comparison with the analytical solution for a 1D slab. In addition the inclusion of the narrow band cK description has been validated in comparison with the line-by-line solution. The participating medium is either grey gas ($\kappa = 1\ m^{-1}$), H_2O or CO_2 . In all the specified cases, walls are black ($\varepsilon_w = 1$). Two different temperature profiles are considered:

$$\text{parabolic:}\quad T_m = 500 - 2000x^2 + 2000x\ K,\quad T_{w1} = T_{w2} = 500\ K.$$

$$\text{linear:}\qquad T_m = 500 + 1000x\ K,\quad T_{w1} = 500\ K,\quad T_{w2} = 1500\ K.$$

Figure 1 shows plots of different cases proving the validity of the Monte Carlo narrow band correlated-K solver used.

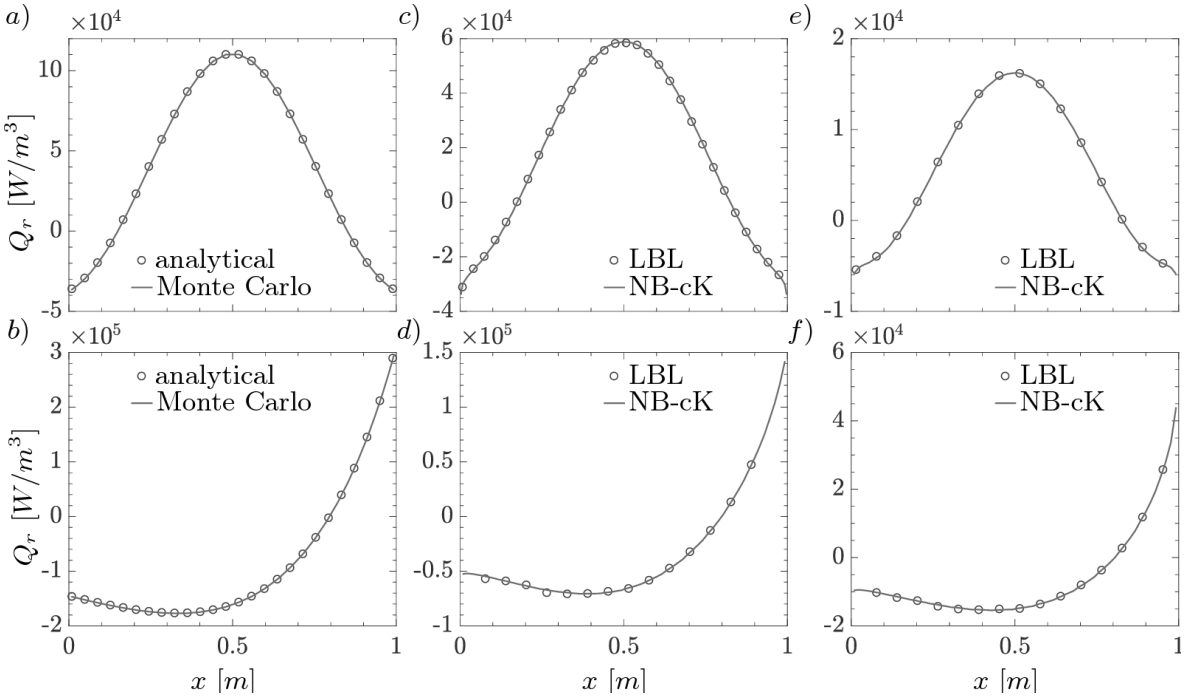

Figure 1: Validation for non-isothermal temperature profiles. Comparison with analytical solution for grey gas and with line-by-line solution for real gas. (a): grey gas, parabolic profile; (b): grey gas, linear profile; (c): H_2O, parabolic profile; (d): H_2O, linear profile; (e): CO_2, parabolic profile; (f): CO_2 , linear profile.

RESULTS

The results of the non-grey simulations are compared with DNS of grey gas performed with FVM and $\kappa = f(T)$, modelled as the Planck mean absorption coefficient of water vapour $\kappa_P^* = C_k(c_0 + c_1\gamma + c_2\gamma^2 + c_3\gamma^3 + c_4\gamma^4 + c_5\gamma^5)$, where $\gamma = A/T^*$. Coefficients $c_0 - c_5$ and A have been taken from Sandia National Laboratories [15]. C_k is a parameter that enables the tuning of the optical thickness of the channel, defined as $\tau = (2\delta)^{-1}\int_0^{2\delta}\overline{\kappa}_P dy$. The three target optical thicknesses are $\tau = 0.1,\ 1$ and 10. In order to properly analyze the effect of TRI, the radiative power per unit volume is divided into an emissive power and an absorptive power as

$$Q_r = Q_e - Q_a$$

where

$$Q_e = \underbrace{\frac{\int_0^\infty \kappa_\lambda I_{b,\lambda} d\lambda}{\int_0^\infty I_{b,\lambda} d\lambda}}_{\kappa_P} \underbrace{4\int_0^\infty I_{b,\lambda} d\lambda}_{E_m}, \quad Q_a = \int_0^\infty \kappa_\lambda \frac{1}{\pi}\int_{4\pi} I_\lambda d\Omega d\lambda$$

E_m is here called emission. In order to have a variable to compare to E_m , also absorptive power is decomposed as $Q_a = \kappa_P G$ where G is here called incident radiation. We note that for the grey gas cases G is the real incident radiation, while for the case with non-grey radiation (H_2O) it is a convenient reference quantity.

Mean profiles

Figures 2(a) and 2(b) show the profiles of Favre averaged non-dimensional temperature $\widetilde{\theta}$ and Reynolds averaged divergence of radiative heat flux $\overline{Q_r}$ (the inlay shows a zoom on the y-axis). The profiles of mean temperature in figure 2(a) show, for the grey cases, the same trend as already observed in [1] for constant κ, namely, the bulk temperature increases drastically with the inclusion of radiative heat transfer, with an overall rise in temperature gradient in the core of the channel upon increasing optical thickness. Surprisingly, despite the fact that the Planck mean optical thickness for the H_2O case is relatively close to $\tau = 10$ ($\tau = 8.026$), the temperature profile is noticeably different, having a lower gradient in the core and a larger gradient close to the walls. Moreover, the mean radiative heat source, figure 2(b) is very similar to the $\tau = 1$ case, with the local maximum/minimum located closer to the wall. Therefore, the introduction of a real gas spectrum, characterized by a high absorption coefficient variability, strongly impacts the heat transfer in the channel, modifying the profiles in a non-intuitive manner. This modification can be further investigated with the analysis of temperature variance and fluctuations of radiative quantities.

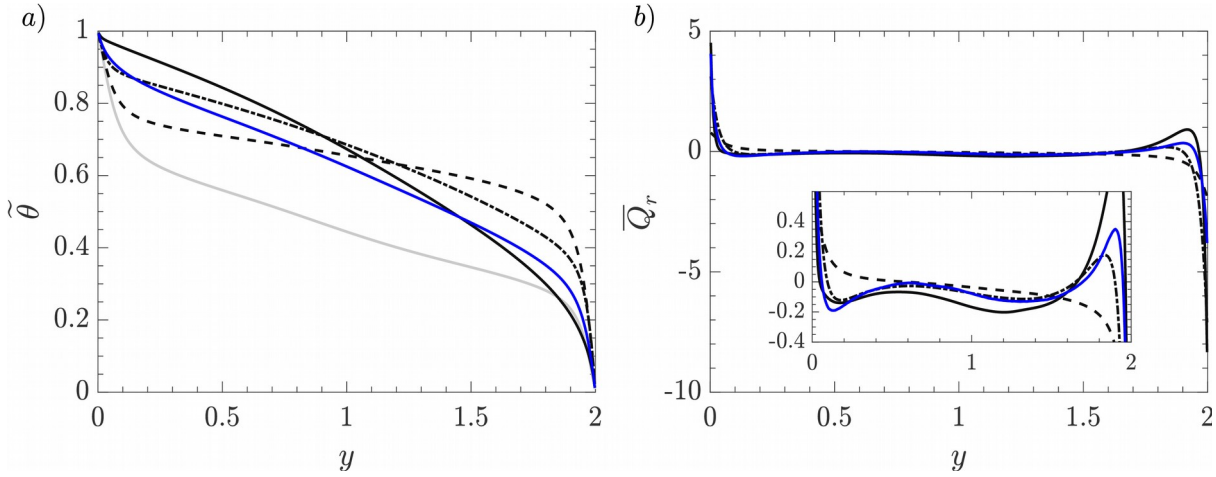

Figure 2: Averaged profiles, grey solid line: no radiation, dashed line: $\tau = 0.1$, dashed-dotted line: $\tau = 1$, black solid line: $\tau = 10$, blue solid line: H_2O ($\tau = 8.026$). (a): mean temperature; (b): mean radiative heat source (the inlay shows a zoom on the y-axis around $Q_r = 0$).

Temperature variance and fluctuations of radiative quantities

Figure 3 shows temperature root mean square profiles for all cases. The temperature root mean square profile changes drastically with the inclusion of radiative heat transfer, proving that TRI heavily influences temperature structures in a radiative turbulent flow. Reminding what has been pointed out in [10], the direct influence of radiative heat transfer on θ' can be divided into an "Emission dissipation" ($\overline{E'_m\theta'}$) and an "absorption source" ($\overline{G'\theta'}$). While the first one is always tightly coupled with θ' and acts proportionally to mean temperature and mean absorption coefficient, the second grows drastically with an increase of optical thickness and acts preferentially on larger, more "optically thick", temperature structures. Differently from a grey gas, in the present cases the absorption term can also act as a sink of temperature fluctuations, since the correlation between temperature and absorption coefficient is negative. Indeed the effect of radiation for a low optical thickness ($\tau = 0.1$) consists in a dissipation of temperature fluctuations in the core of the channel, where a lower production combined with the action of emission dissipation causes a destruction of temperature variance. On the other hand, a recovery of temperature fluctuations in the center of the channel, where large temperature structures are located, is noticeable for a large optical thickness, while temperature variance is destroyed near the walls where temperature fluctuations are characterized by large anisotropy and and a smaller length scale. This shows the effect of the wavenumber dependency of the "absorption source". All these results fit well the theory described in [10], while the temperature fluctuations for the H_2O case seem to not follow the same trend. In particular, for a $\tau = 8.026$, lower than the $\tau = 10$ case, a temperature fluctuation recovery can be noticed in virtually all the channel when compared to the $\tau = 1$ case, not only in the presence of large isotropic structures as it could have been predicted. This could suggest that the behaviour of the absorption source, which influences the qualitative effect of TRI (i.e. which scales are affected in which zones of the channel), is similar to a grey gas with $\kappa > \kappa_P$ (i.e., radiative length scales are shorter than for the $\tau = 10$ case). On the other hand, the magnitude of the recovery is still lower, in the core, when compared to the $\tau = 10$ case. This could seem non-intuitive since it suggests that the "qualitative" behaviour of TRI, connected to the length scales of radiative transfer, is disconnected from the "quantitative" magnitude (i.e., the quantification of the impact of radiation on θ'), whereas in all the other cases they are linked together (i.e., smaller radiative length scales correspond to a larger impact of TRI on θ').

Recalling the introduction, from the grey gas analysis it is concluded that in a grey gas for a small κ, $Q'_r \propto E'_m \gg G'$, while for a large κ $Q'_r \propto E'_m - G' \ll E'_m \approx G'$. This behaviour is different when considering a real spectrum.

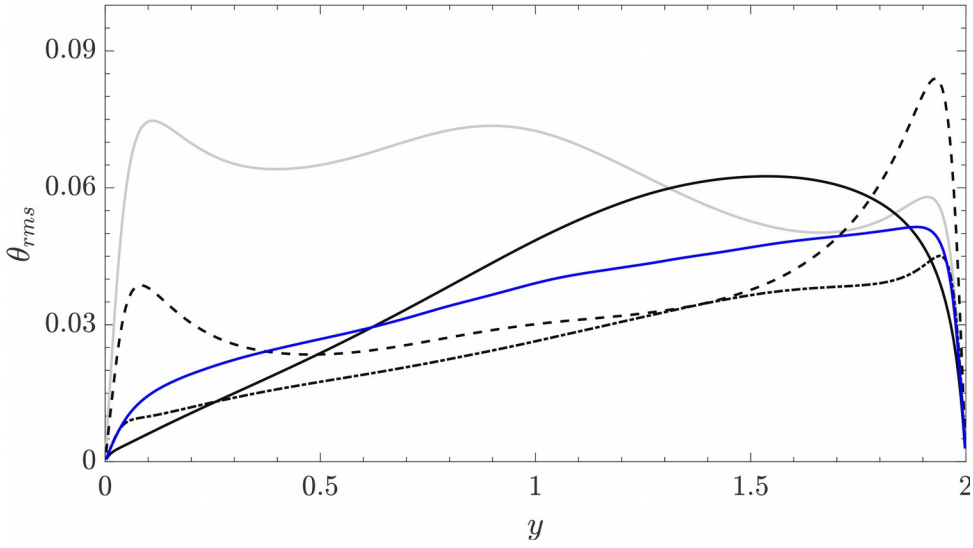

Figure 3: intensity of temperature fluctuations, grey solid line: no radiation, dashed line: $\tau = 0.1$, dashed dotted line: $\tau = 1$, black solid line: $\tau = 10$, blue solid line: H_2O ($\tau = 8.026$).

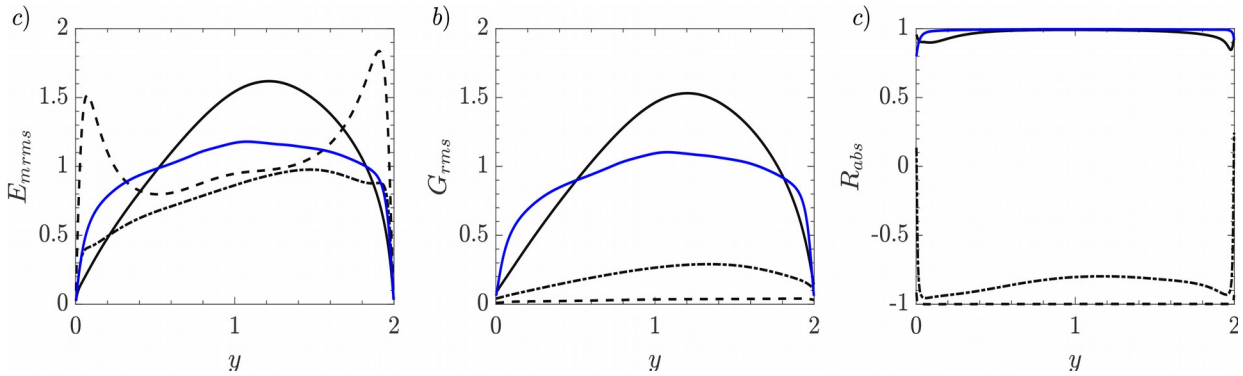

Figure 4: root mean square profiles of emission (a) incident radiation (b) and absorption power-temperature correlation (c), dashed line: $\tau = 0.1$*, dashed dotted line:* $\tau = 1$*, black solid line:* $\tau = 10$*, blue solid line:* H_2O $\tau = 8.026$.

Figures 4(a) and (b) show profiles of $E_{m,rms}$ and G_{rms}, respectively, confirming what has been noticed in figure 3. In particular for the H_2O case:

a) $E_{m,rms}$ and G_{rms} have a comparable magnitude, which is typical of a high optical thickness channel;
b) G_{rms} are larger than for $\tau = 10$ near the walls, which shows that absorption acts also on smaller temperature structures behaving as if $\tau > 10$ (shorter radiative length scales);
c) the overall magnitude of $E_{m,rms}$ and G_{rms} is smaller than for $\tau = 10$, which, on the contrary, would imply that $\tau < 10$.

In particular, the large κ behaviour ($Q'_r \propto E'_m - G' \ll E'_m \approx G'$) can be recognized at lower κ, therefore with a lower magnitude. A further proof of point b) comes from the analysis of absorption power/temperature correlation, defined as

$$R_{abs} = \frac{\overline{Q'_a \theta'}}{Q_{a,rms}\theta_{rms}}$$

This quantity is constrained between -1 and 1, being negative if positive temperature fluctuations cause negative absorptive power fluctuations and positive vice versa. The magnitude of R_{abs} represents the locality of Q_a fluctuations. If R_{abs} is large in magnitude ($\approx \pm 1$), all absorptive power fluctuations are caused by local temperature change. On the other hand, a low R_{abs} magnitude (≈ 0) signifies that Q'_a is caused by non-local effects. Taking into account the absorptive power decomposition, R_{abs} can be calculated as

$$R_{abs} = \frac{\overline{\kappa_P} \cdot \overline{G'\theta'}}{Q_{a,rms}\theta_{rms}} + \frac{\overline{G} \cdot \overline{\kappa'_P \theta'}}{Q_{a,rms}\theta_{rms}} + \frac{\overline{\kappa'_P G'\theta'}}{Q_{a,rms}\theta_{rms}}$$

It has to be noticed that the third term in the numerator is a third order term and thus can be neglected, while the second term is always negative (κ_P decreases with an increase in θ) and the first term is always positive (a higher temperature signifies larger amount of energy to absorb). R_{abs} is displayed in figure 4(c). For $\tau = 0.1$ and $\tau = 1$ the numerator in equation 5.3 is dominated by $\overline{\kappa'_P \theta'}$, while, as radiative length scales shorten, G becomes local and a tight coupling between temperature and incident radiation fluctuations can be noticed. It is interesting to notice that, despite the lower τ, R_{abs} is larger for the H_2O case when compared to the $\tau = 10$ case, proving the presence of a shorter radiative length scale in the first with respect to the latter case.

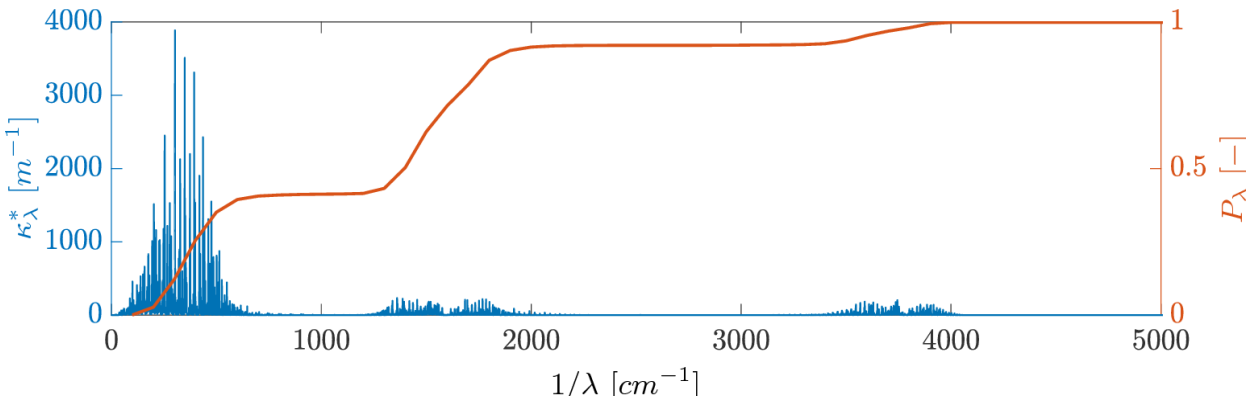

Figure 5: Left axis: absorption spectrum of H_2O at $750\ K$. Right axis: cumulative probability associated with the spectral emission at $750\ K$, $P_\lambda = \int_0^\lambda \kappa_\lambda I_{b,\lambda} d\lambda / \int_0^\infty \kappa_\lambda I_{b,\lambda} d\lambda$

ANALYSIS AND CONCLUDING REMARKS

The evidence shown allows to distinguish two different aspects of TRI, which in previous grey gas results (present work, [1]) are not separable. The first one is the impact of TRI on temperature fluctuations (i.e., the influence of radiative term over other temperature variance budgets), here termed "quantitative" TRI, the second aspect regards the shapes of the profiles and the preferential impact of TRI on different scales of the temperature field and it is here called "qualitative" TRI.

As already described in Silvestri et al. (2017), the dual mechanism of TRI consists in a withdrawal of energy at all scales due to emission and a redistribution of energy on large temperature structures caused by absorption. Therefore, it is clear that the quantitative TRI is linked to the amount of emitted power, since this sets the amount of energy available for absorption.

On the other hand, the qualitative TRI is connected to the length scale of radiative heat transfer (i.e., how far a ray can travel), and thus linked to incident radiation. In a grey gas, the two are connected since both incident radiation and emission are defined by the same absorption coefficient, therefore, the higher the emitted power, the lower the radiative length scale. This leads to the tight connection of qualitative and quantitative effects.

When the participating media, on the other hand, is characterized by a real gas spectrum, as highly variable as the one of water vapour, the two effects decouple, because of the different relevance of different spectral wavelengths. Water vapour's spectral absorption coefficient, in the range of $500 - 1000\ K$, has values as high as $4000\ m^{-1}$ (see figure 5). Indeed it has been already proven that an increase of absorption coefficient causes an increase in incident radiation fluctuations (see figure 4(b)). Therefore, the largest share of incident radiation fluctuations, which define the qualitative TRI, will be associated to the spectral lines corresponding to the highest absorption coefficients. In the major 3 emission bands (represented by a larger gradient in the cumulative probability function in figure 5) the latter are ~ 4000, ~ 250 and $\sim 210\ m^{-1}$. On the other hand, the Planck mean absorption coefficient is everywhere lower than $20\ m^{-1}$. Therefore, the "absorption coefficient" associated with incident radiation fluctuations and "qualitative" TRI is effectively much higher than the one associated with emission and "quantitative" TRI. This explains the discrepancy noticed between the grey cases and the real gas case and explains why a real gas behaves as a grey gas with $\kappa \gg \kappa_P$.

REFERENCES

1. A. Gupta, M.F. Modest and D.C. Haworth, “Large-eddy simulation of turbulence radiation interactions in a turbulent planar channel flow”. *J. Heat Transfer 131 (6),* 2009, 061704
2. K.V. Deshmukh, M.F. Modest and D.C. Haworth, “Direct numerical simulation of turbulence-radiation interactions in a statistically one-dimensional nonpremixed system”. *J. Quant. Spectrosc. Radiat. Transfer 109*, 2391 – 2400, 2008.
3. P.J. Coelho, O.J. Teerling and D.J.E.M. Roekaerts, “Spectral radiative effects and turbulence/radiation interaction in a non-luminous turbulent jet diffusion flame”. *Combustion and Flames 133*, 75 – 91, 2003
4. L. Tesse, F. Dupoirieux and J. Taine “Monte Carlo modeling of radiative transfer in a turbulent sooty flame”. *Int. J Heat Mass Transfer 47*, 555 – 572, 2004
5. M. Roger, P.J. Coelho and C.B. da Silva “Relevance of subgrid-scales for large eddy simulations of turbulence-radiation interactions in turbulent planar jet”. *J. Quant. Spectrosc. Radiat. Transfer 112*, 1250 – 1256, 2011
6. A. Sakurai, K. Matsubara, K. Takakuwa and R. Kanbayashi, “Radiation effects on mixed turbulent natural and forced convection in a horizontal channel using direct numerical simulation”. *Int. J. Heat Mass Transfer 55*, 2539 – 2548, 2010
7. R. Vicquelin, Y.F. Zhang, O. Gicquel and J. Taine, “Effects of radiation in turbulent channel flow: analysis of coupled direct numerical simulations”. *J. Fluid Mech. 753,* 360 – 401, 2014
8. S. Ghosh and R. Friedrich, “Effects of radiative heat transfer on the turbulence structure in inert and reacting mixing layers”. *Phys. Fluids 27*, 055107, 2015
9. S. Ghosh, R. Friedrich, M. Pfitzner, C. Stemmer, B. Cuenot and M. el Hafi, “Effects of radiative heat transfer on the structure of turbulence supersonic channel flow”. *J. Fluid Mech. 677*, 416 – 444, 2011
10. S. Silvestri, A. Patel, D.J.E.M. Roekaerts and R. Pecnik, “Turbulence Radiation Interaction in channel flow with various optical thickness”. *J. Fluid Mech. 834, 359 – 384,* 2018
11. A. Patel, J.W.R. Peeters , B.J. Boersma and R. Pecnik, “Semi-local scaling and turbulence modulation in variable property turbulent channel flows”. *Phys. Fluids* 27 (7), doi:10.1063/1.4929813, 2015
12. B.J. Boersma, “A 6th order staggered compact finite difference method for the incompressible Navier-Stokes and scalar transport equations”. *J. Comput. Physics* 230, 4940 – 4954, 2011
13. Y.F. Zhang, O. Gicquel and J. Taine, “Optimized Emission-based Reciprocity Monte Carlo Method to speed up computation in complex systems”. *Intl J. Heat Mass Transfer* 55 (25), 8172-8177, 2012
14. L.S. Rothman et al, “The HITRAN2012 molecular spectroscopic database”. *J. Quant. Spectrosc. Radiat. Transfer* 130, 4-50
15. Web site for the International Workshop on Measurement and Computation of Turbulent Non premixed Flames (TNF), R. S. Barlow, Ed., Sandia National Laboratories, http://www.sandia.gov/TNF/radiation.html